www.acsnano.org

Sub-3-Nanometer Domain Spacings of Ultrahigh- χ Multiblock Copolymers with Pendant Ionic Groups

Jinseok Park, Anne Staiger, Stefan Mecking, and Karen I. Winey*



Downloaded via CORNELL UNIV on October 22, 2021 at 14:28:42 (UTC). See https://pubs.acs.org/sharingguidelines for options on how to legitimately share published articles.

Cite This: https://doi.org/10.1021/acsnano.1c06734



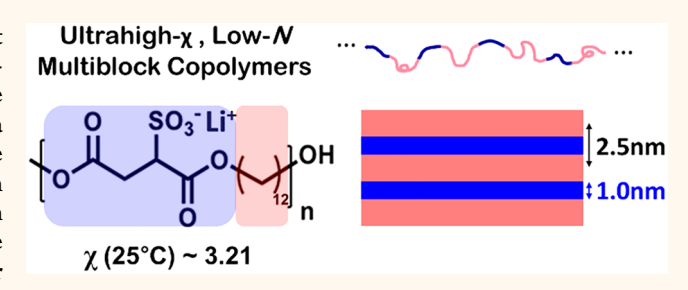
ACCESS

Metrics & More

Article Recommendations

Supporting Information

ABSTRACT: We investigated the temperature-dependent phase behavior and interaction parameter of polyethylene-based multiblock copolymers with pendant ionic groups. These step-growth polymers contain short polyester blocks with a single Li^+SO_3^- group strictly alternating with polyethylene blocks of x-carbons (PESxLi, x=12,18,23). At room temperature, these polymers exhibit layered morphologies with semicrystalline polyethylene blocks. Upon heating above the melting point ($\sim 130~^\circ\text{C}$), PES18Li shows two order-to-order transitions involving Ia3d gyroid and hexagonal morphologies.



For PES12Li, an order-to-disorder transition accompanies the melting of the polyethylene blocks. Notably, a Flory–Huggins interaction parameter was determined from the disordered morphologies of PES12Li using mean-field theory: $\chi(T) = 77.4/T + 2.95$ (T in Kelvin) and $\chi(25\,^{\circ}\text{C}) \approx 3.21$. This ultrahigh χ indicates that the polar ionic and nonpolar polyethylene segments are highly incompatible and affords well-ordered morphologies even when the combined length of the alternating blocks is just 18–29 backbone atoms. This combination of ultrahigh χ and short multiblocks produces sub-3-nm domain spacings that facilitate the control of block copolymer self-assembly for various fields of study, including nanopatterning.

KEYWORDS: multiblock copolymer, high-χ block copolymer, ion-containing polymer, self-assembly, phase diagram, nanopatterning

tilization of self-assembled materials is an essential technology for producing nanostructured materials such as nanowires, 1,2 nanodots, 3,4 and nanoporous ⁻⁷ Nanostructured materials made by using selfassembled templates of various shapes and length scales exhibit a wide variety of material properties that enable new applications for semiconductors, 8,9 metamaterials, 10,11 and 2D materials. 12-14 Among the various templating materials, block copolymers have emerged as exceptionally versatile materials, as they can self-assemble into ordered nanostructures with sub-10-nm feature sizes. 15 More recently, many studies have contributed to developing the block copolymers with smaller feature sizes particularly focused on transferring nanopatterns for microelectronic devices. 16,17 Synthetically, the underlying mechanism of controlling the domain spacing (d) of block copolymers is a well-known scaling to the Flory-Huggins interaction parameter (χ) and degree of polymerization (N). For linear and symmetric diblock copolymers, d exhibits weaker χ -dependency (e.g., $d \sim \chi^{1/6} N^{2/3}$ for strongly segregated systems) than the segregation strength (e.g., χN). ^{18–21} Note that we use χ to indicate an effective χ for clarity. Thus, N should be decreased to produce smaller d, while χ should be increased to retain sufficiently strong microphase separation.

Therefore, block copolymers with high χ and low N are a common strategy to reduce and control the feature size of block copolymers.

A variety of high- χ block copolymers have been designed by the addition of chemically incompatible functionalities to either of the blocks. Such incompatibility often arises from the difference of hydrophilicity (or hydrophobicity) between the blocks. For example, with the addition of a hydroxyl group to one styrene block, a poly(4-hydroxystyrene-b-styrene) diblock copolymer self-assembles into a layered morphology with d=11.8 nm and χ (170 °C) \approx 0.12. With the addition of one more hydroxyl group, poly(3,4-dihydroxystyrene-b-styrene) exhibits a layered morphology with d=5.9 nm and χ (170 °C) \approx 0.46. Similarly, introducing hydrophobic functionalities increases the incompatibility between the blocks, such as

Received: August 5, 2021 Accepted: October 4, 2021



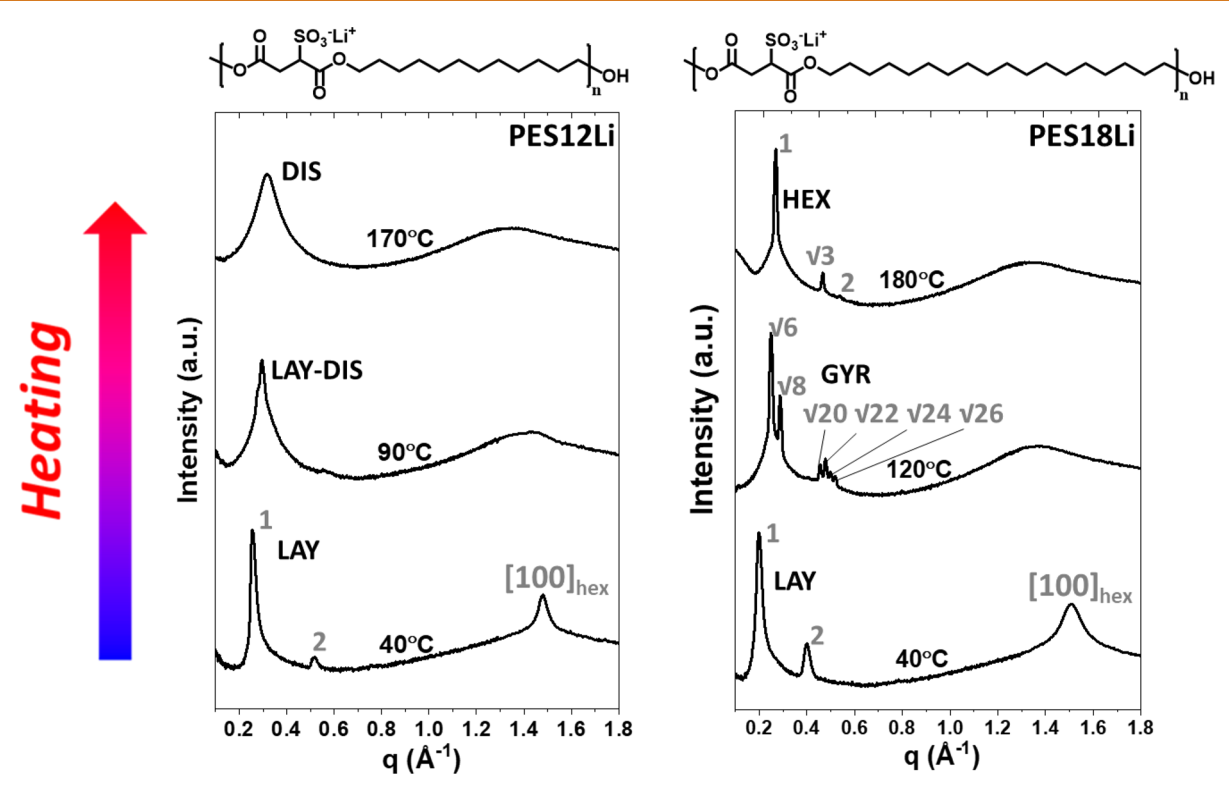


Figure 1. In situ X-ray scattering of PES12Li and PES18Li at selected temperatures upon heating. At $q < 0.8 \text{ Å}^{-1}$, LAY, DIS, GYR, and HEX represent layered, disordered, gyroid, and hexagonally packed cylinder morphologies of ionic aggregates. The peak at $q \approx 1.5 \text{ Å}^{-1}$ indicates the crystalline polyethylene backbone below $T_{\rm m}$.

silicon-containing $^{24-26}$ and fluoroalkyl groups. 27,28 Specifically, poly(3-hydroxystyrene-b-dimethylsiloxane) 24 shows a layered morphology with d=7.4 nm and $\chi(170~^{\circ}\mathrm{C})\approx0.39$, and poly(3-hydroxystyrene-b-pentadecafluorooctyl methacrylate) 27 has d=9.8 nm for layers and $\chi(170~^{\circ}\mathrm{C})\approx0.48$. These χ parameters are obtained from the X-ray scattering intensity of disordered diblock copolymer melts and mean-field theory and are scaled to the common reference volume of 118 Å $^{3.16}$ Note that the conventional poly(styrene-b-methyl methacrylate) diblock copolymer has a relatively low $\chi(170~^{\circ}\mathrm{C})\approx0.038$, limiting the minimum feature size to $\sim\!20$ nm. 29

A multiblock architecture, such as an (AB), linear multiblock copolymer, is a promising candidate for designing high- χ and low-N polymers due to their ability to microphase separate into ordered microstructures and tunability of physical properties. 30,31 In strictly alternating (AB)_n multiblock copolymers, an increasing number of repeating subunits (n) results in smaller domain spacings than AB diblock copolymers.^{32–34} This is due to the reduced chain-end effects in multiblock copolymers relative to diblock copolymers. Also, the multiblock architecture is critical for preparing high-y and low-N polymers, because the thermal and mechanical properties of diblock copolymers are significantly compromised at very low $N.^{35-37}$ Therefore, (AB), linear multiblock copolymers are promising as a route to achieving sub-10-nm domain spacings with thermal and mechanical stability.

However, microphase separation of (AB)_n symmetric linear multiblock copolymers requires a higher segregation strength with increasing n, as $\chi N > 10.5$ for n = 1 (equivalent to diblock copolymers) and $\chi N > 15.1$ for $n > 20.^{38}$ Note that the N of an (AB)_n multiblock copolymer corresponds to the degree of polymerization of the AB subunit. As n reaches ~ 20 , the phase behavior is dictated by the χ and N as the influence of n

becomes negligible.^{38–40} Similarly, the domain spacing of the multiblock copolymer is independent of n at large n.³³ Therefore, $\chi N > 15.1$ is required for high- χ and low-N polymers with $(AB)_n$ multiblock architectures to exhibit strong microphase segregation.

Ion-containing polymer systems are a promising strategy for preparing high- χ multiblock copolymers, because the presence of ionic groups effectively increases the segregation strength between the blocks. 16,41–44 For example, our previous studies examined the phase behaviors of polyethylene-based sodium sulfosuccinate (PESxNa) multiblock copolymers, which contain short polar blocks with pendant Na⁺SO₃⁻ groups and nonpolar polyethylene blocks of x carbons (x = 10-48). 45-47 Notably, these ion-containing multiblock copolymers microphase separate into ordered morphologies such as lamellar, gyroid, and hexagonally packed cylinder morphologies, and the smallest domain spacing is ~2.2 nm in the lamellar and hexagonal morphologies of PES10Na. These results suggest that the nonpolar polyethylene blocks are highly incompatible with the polar ionic blocks, indicating a high χ in these PESxNa polymers. However, the γ of PESxNa was experimentally inaccessible due to the absence of disordered morphologies below the polymer degradation temperature.

This study of PESxLi multiblock copolymers (x = 12, 18, 23) demonstrates sub-3-nm ordered microstructures and an ultrahigh Flory–Huggins interaction parameter (χ). These polymers are strictly alternating multiblock copolymers synthesized from the step-growth polymerization of short polar and nonpolar polyethylene blocks. For PES18Li, various order-to-order transitions between layered, gyroid, and hexagonally packed cylinder morphologies are observed, and the domain spacings of layered and hexagonal morphologies are 3.2 and 2.3 nm, respectively. In addition, PES12Li has a

layer spacing of 2.5 nm and an accessible order-to-disorder transition. The random phase approximation was applied to the disordered PES12Li using a reference volume of 118 Å³ to determine $\chi(T)=77.4/T+2.95$. This ultrahigh χ for the PES12Li multiblock copolymer is consistent with the strong segregation of short ionic blocks and ordered morphologies with sub-3-nm domain spacings and demonstrates an approach for designing high- χ and low-N copolymers.

RESULTS AND DISCUSSION

High- χ and low-N block copolymers are typically synthesized by anionic polymerization to tightly control the block molecular weights and thus the self-assembled morphologies. In contrast, the PESxLi multiblock copolymers have broader molecular weight distributions, because they are synthesized via step-growth polymerization, which affords a wider range of monomeric units than anionic polymerization. The polydispersity indexes of PES12Li and PES18Li are nominally ~1.43 and ~1.24, respectively (Figure S1). Importantly, the polar and nonpolar monomeric units in PESxLi are chemically precise and strictly alternating and thus produce well-defined selfassembled morphologies. The number of repeating units (n) of the PESxLi multiblock copolymers was determined by the end group analysis of ${}^{1}H$ NMR signals (Figures S2 and S3): n = 55for PES12Li and n = 17 for PES18Li. Note that the value of nis proportional to the total molecular weights of PESxLi polymers and remains constant during the cation exchange of the polymers.⁴⁷

In situ X-ray scattering experiments at selected temperatures show various morphologies of PES12Li and PES18Li (Figure 1). The X-ray scattering data at all measured temperatures for heating and cooling and differential scanning calorimetry (DSC) results are provided in the Supporting Information (Figures S4 and S5). At 40 °C, PES12Li and PES18Li exhibit layered (LAY) ionic aggregate morphologies as indicated by the peak ratio (q/q^*) of 1:2 at $q < 0.8 \text{ Å}^{-1}$. These LAY morphologies coexist with the [100] plane of hexagonally packed crystalline polyethylene, as evidenced by a peak at $q \approx$ 1.5 Å⁻¹. Note that homopolyethylene forms orthorhombic crystals at ambient condition, 48 while the short polyethylene blocks alternating with polar ionic blocks of PESxLi form hexagonal crystals. The domain spacing of these layered morphologies (d_L) increases with the polyethylene block lengths, and $d_L = 2\pi/q^* = 2.5$ and 3.2 nm for PES12Li and PES18Li, respectively.

Heating above the melting temperature leads to a broad amorphous halo centered at $q \approx 1.5 \text{ Å}^{-1}$ for both polymers, and the LAY morphologies transition into a disordered morphology (DIS) for PES12Li and gyroid (GYR) morphology for PES18Li. For PES12Li, the q^* peak transitions into a broad single peak at $q \approx 0.3 \text{ Å}^{-1}$ and indicates an order-todisorder transition. In contrast, PES18Li exhibits an order-toorder transition from a LAY to a GYR morphology, which is assigned by the observed peak ratios (q/q^*) of $\sqrt{6}:\sqrt{8}:\sqrt{20}:\sqrt{22}:\sqrt{24}:\sqrt{26}$. A further increase of temperature in PES18Li produces a transition from GYR to hexagonally packed cylinder (HEX) morphology, as indicated by the observed peak ratio of 1: $\sqrt{3}$:2. These peaks are not overlapping with the local minimum of the corresponding cylinder form factor. At 180 °C, the lattice parameter of the HEX morphology of PES18Li is 2.7 nm. Notably, ordered morphologies in these polymers form sub-3-nm domain

spacings with relatively short lengths of polar ionic and nonpolar polyethylene blocks.

Upon *in situ* cooling, X-ray scattering shows that PES12Li maintains DIS morphologies to 40 °C, while PES18Li shows the HEX–GYR transition and then the GYR morphologies persist until 40 °C (Figures S4 and S5). The absence of recrystallization in these polymers is attributed mainly to the strong polar interactions that slow the crystallization kinetics. Similar behavior was previously observed with the sodium sulfonate multiblock copolymers (PESxNa) in our previous studies. The morphological transitions characterized by X-ray scattering experiments are consistent with the thermal transitions observed in the DSC (Figures S4 and S5).

Figure 2 shows the heating morphology map of PESxLi as a function of temperature and volume fraction of polar blocks

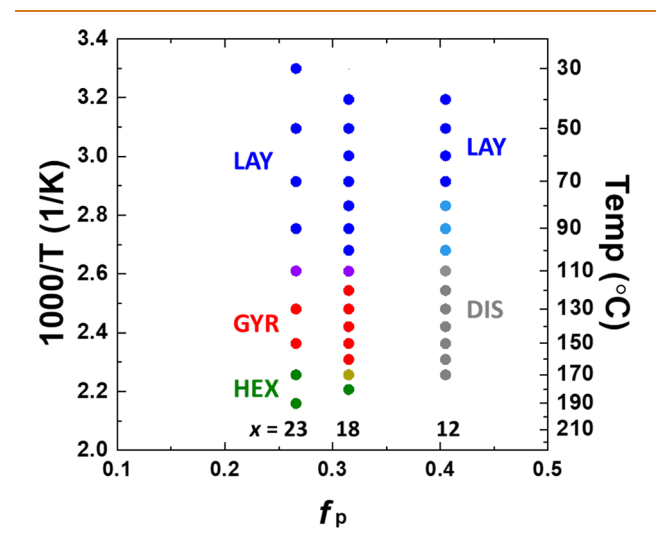


Figure 2. Morphology map of PESxLi polymers as a function of temperature and $f_{\rm p}$, the volume fraction of the polar block. The morphologies are determined from the heating cycle of *in situ* X-ray scattering experiments. The morphology transitions are shown as purple (LAY–GYR), olive (GYR–HEX), and light blue (LAY–DIS). The PES23Li data are obtained from ref 46.

 $(f_{\rm p}).$ The value of $f_{\rm p}$ is calculated from the ratio of van der Waals volume of the blocks. The PES23Li data were previously reported. With increasing temperatures, LAY–GYR–HEX order-to-order transitions are observed for PES23Li and PES18Li at the $f_{\rm p}$ of 0.27 and 0.31, respectively. Due to the degradation of the polymers, a DIS morphology of PES18Li and PES23Li was inaccessible. In contrast, PES12Li $(f_{\rm p}=0.41)$ exhibits an order-to-disorder transition (LAY–DIS) with increasing temperature. This morphology map directly compares the effect of block lengths and temperature on the segregation strength (χN) since $\chi\sim 1/T$ and $N\sim 1/f_{\rm p}.$ Here, the segregation strength decreases with higher T or higher $f_{\rm p}$, leading to the DIS morphologies in PES12Li.

For PES12Li, a wide LAY–DIS transition window at 80–100 °C is associated with the melting temperature ($T_{\rm m}\approx73$ °C) and order-to-disorder transition temperature ($T_{\rm ODT}\approx112$ °C); see Figure 3S(b) for DSC results. At 80–90 °C, an amorphous polyethylene backbone leads to the poorly defined LAY morphologies. Following an isothermal anneal at 90 °C for 20 h, the amorphous LAY morphology is evident with a weak second-order peak (Figure S6). The interlayer distance with amorphous polyethylene blocks is just 2.1 nm compared

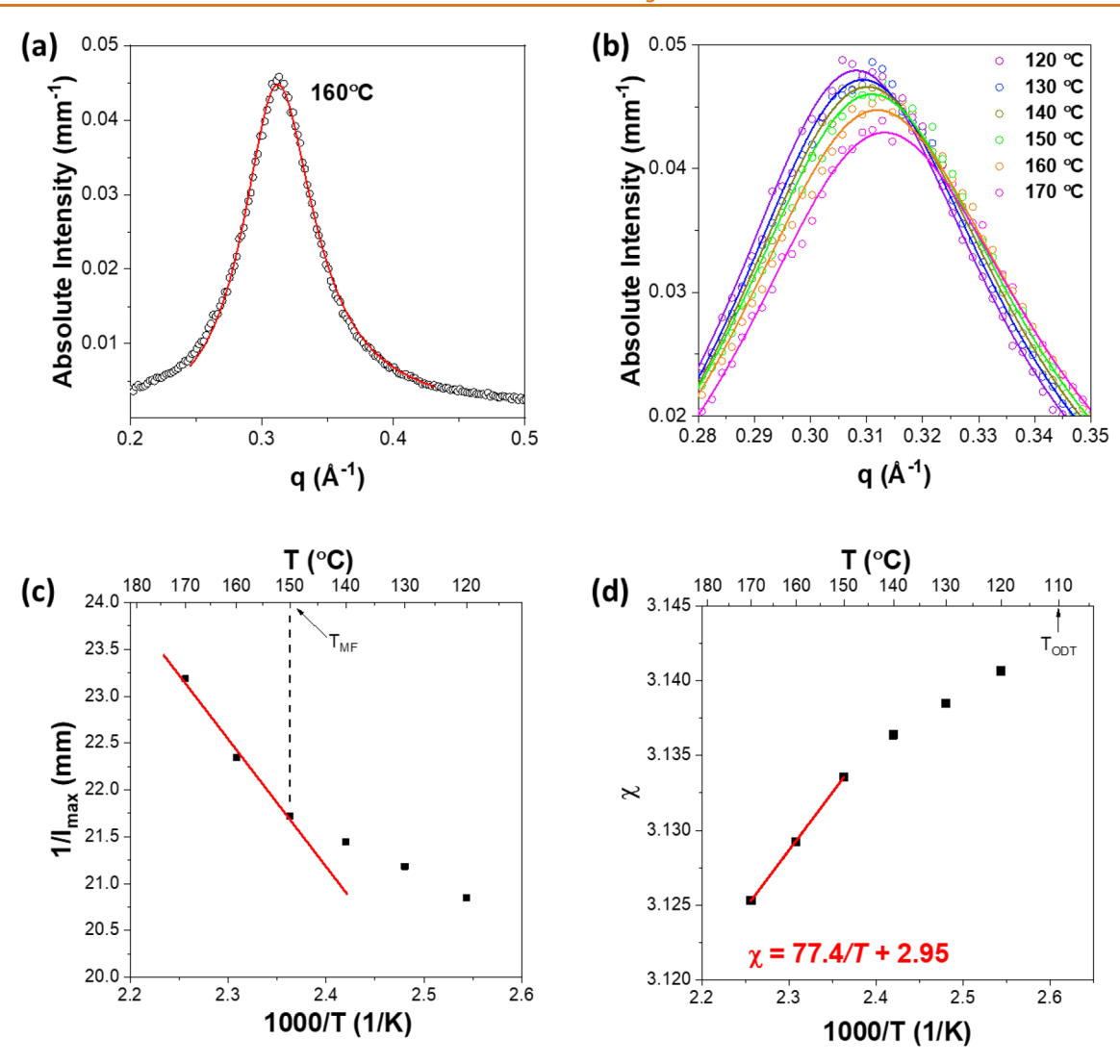


Figure 3. (a) Scattering intensity of disordered PES12Li at 160 °C (dots) and the best fit of eq 1 (line). (b) Scattering intensity (dots) and eq 1 (line) every 10 °C from 120 to 170 °C. Fitting parameters are provided in Table S1. (c) $1/I_{\rm max}$ vs 1/T plots, where $I_{\rm max}$ is the absolute scattering intensity at q^* . The red line shows the linear relationship between $1/I_{\rm max}$ and 1/T above the mean-field temperature $(T_{\rm MF})$. (d) χ vs 1/T plots and its linear fit above the $T_{\rm MF}$. The value of χ is determined from the fitting shown in (b).

to the crystalline polyethylene (2.5 nm at 40 °C). The LAY morphologies below $T_{\rm m}$ possess crystalline polyethylene blocks, while at 90 °C the melting of polyethylene reduces the backbone ordering and the interlayer spacing between the ionic aggregate layers. At a higher temperature, an order-to-disorder transition at ~110 °C is identified with a non-Lorentzian, broad single peak in X-ray scattering at $q\approx 0.3$ Å⁻¹. Therefore, the morphology map for a given in situ X-ray scattering experiment observes a relatively wide range of LAY—DIS transitions in PES12Li.

The effective Flory–Huggins interaction parameter (χ) of PESxLi is calculated using a random phase approximation of $(AB)_n$ multiblock copolymers with a volume-based degree of polymerization and reference volume of 118 Å^{3.38} The X-ray scattering intensity from the disordered $(AB)_n$ multiblock copolymers are defined as $I(q) = \frac{C}{1/i(q)-2\chi}$ at $n \to \infty$, where C is a constant and i(q) is the intensity per repeating unit. The quantity i(q) is

$$i(q) = N_{\nu} f_{p}^{2} (1 - f_{p})^{2}$$

$$\times \left[\frac{2}{\lambda f_{p} (1 - f_{p})} - \frac{2(1 - e^{-\lambda f_{p}})(1 - e^{-\lambda (1 - f_{p})})}{\lambda^{2} f_{p}^{2} (1 - f_{p})^{2} (1 - e^{-\lambda})} \right]$$
(1)

where $\lambda=q^2R_{\rm g}^2$, and $R_{\rm g}$ is the radius of gyration of the repeating unit. The i(q) asymptotically converges as n approaches 20. Therefore, the scattering intensities of disordered PES12Li ($n\approx55$ from the NMR end-group analysis) at 120 to 170 °C are fit with eq 1 and the fitting variables of C, χ , and $R_{\rm g}^2$. The volume-based degree of polymerization ($N_{\rm v}$) is calculated from the common reference volume of 118 ų, molecular weight (170 g/mol) and density (0.81 g/cm³) of melt polyethylene block, and $f_{\rm p}$. The scattering profiles and fitting parameters at measured temperatures are provided in Figure S7 and Table S1, respectively.

Figure 3a shows the scattering intensity of disordered PES12Li at 160 °C (dots) and the best fit of eq 1 (line). The quality of fitting at a wide range of q indicates that the mean-field theory accurately calculates the value of γ from disordered

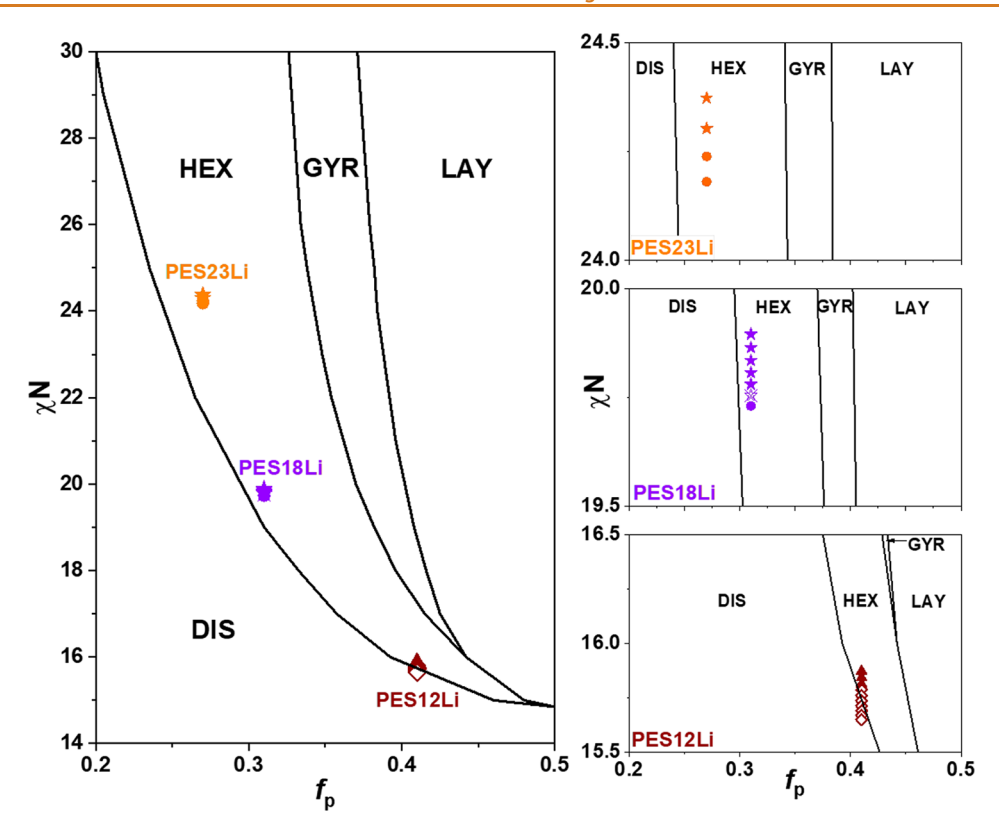


Figure 4. Phase boundaries (lines) of $(AB)_{17}$ multiblock copolymers as determined from the SCFT calculation. Phase behavior of PES12Li (brown), PES18Li (purple), and PES23Li (orange) as a function of χN and f_p , specifically. Symbol shapes indicate the experimentally observed morphologies of the PES χ Li melts: GYR (\star), HEX (\bullet), LAY (\bullet), and DIS (\diamondsuit).

PES12Li. Although the mean-field theory applies to Gaussian conformation, many studies have suggested that the random phase approximation can reasonably approximate the χ parameter with the value of N as low as 10^{16} Figure 3b highlights the maximum scattering intensity (I_{max}) and peak center (q^*) as a function of temperature. With decreasing temperatures, q^* decreases and I_{max} increases, typical of phase behavior in disordered polymer melts. Figure 3c plots $1/I_{max}$ vs 1/T to identify the mean-field temperature $(T_{\rm MF})$ above which the fluctuation effect is negligible. The linear relationship between $1/I_{\rm max}$ and 1/T above $T_{\rm MF} \approx 150$ °C indicates that the disordered phases are consistent with the mean-field calculation. A nonlinear relationship near the order-to-disorder transition temperature is due to the fluctuation effects in disordered polymer melts. 49-51 Therefore, the χ νs 1/T plot gives the $\chi(T) \sim 77.4/T + 2.95$ (*T* in Kelvin) relationship above $T_{\rm MF}$ (Figure 3d).

This $\chi(T)$ relationship indicates that PES12Li exhibits larger enthalpic and entropic contributions to the free energy of mixing than other high- χ diblock copolymers. In these PESxLi polymers, a large enthalpic contribution is attributed to the strong attraction between the charged ionic blocks. A large entropic contribution originates from the stretching energy of short blocks. From this equation, χ at 25 °C is 3.21. In addition, the LAY morphology of PES12Li corresponds to a lattice parameter of 2.5 nm and a feature size (thickness of an ionic layer) of just 1.0 nm. Thus, we demonstrate the ultrahigh χ and sub-3-nm domain spacings of PESxLi multiblock copolymers with pendant ionic groups.

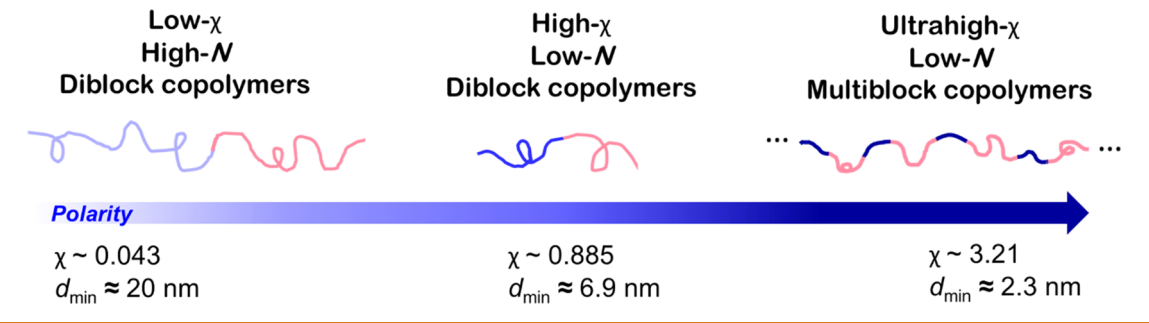
The ultrahigh χ of PES α Li is one of the largest χ values reported for block copolymers¹⁶ and explains the self-assembly of short blocks with sub-3-nm domain spacings. While triblock

architectures have reported high χ values, the explored domain spacings and ordered morphologies were limited. For example, polylactide-poly(dimethylsiloxane)-polylactide triblock copolymers report $\chi(150~^{\circ}\text{C}) \approx 1.06$, while the system identifies the smallest layer spacing of ~20 nm. ⁵³ This may arise from the approximation of χ from the domain spacings, $d \sim N^{2/3} \chi^{1/6}$. Poly(ethylene oxide)-b-perfluoropolyether-b-poly(ethylene oxide) triblock copolymer reported $\chi(30~^{\circ}\text{C}) \approx 3.01$, although no ordered morphologies were observed due to the high volume asymmetry and $\chi N < (\chi N)_{\text{ODT}}$. ⁵⁴ In contrast, PESxLi polymers show both ultrahigh χ and ordered morphologies at sub-3-nm domain spacing.

Various salt-containing block copolymers have been extensively investigated both theoretically and experimentally. Sp-62 In these salt/copolymer systems, the value of χ depends on the salt concentration and solvation energy. For example, poly(styrene-b-ethylene oxide) with lithium bis(trifluoromethane-sulfonyl)imide (LiTFSI) systems observe an increase of χ with salt concentration. In contrast, the χ of PESxLi polymers solely depends on the molecular interactions of the polar and nonpolar blocks. Thus, the current experimental results of the PESxLi system should not be directly compared to the salt/copolymer systems.

The obtained χ and $R_{\rm g}$ values from the random phase approximation are further examined to validate the results. The segregation strength of PES12Li at the $T_{\rm ODT}\approx 112$ °C is $\chi N_{\rm v}\approx 15.8$, which is close to the theoretical segregation limit of $(\chi N)_{\rm ODT}\approx 15.1$ for symmetric multiblock copolymers. A somewhat higher $(\chi N)_{\rm ODT}$ of PES12Li is consistent with the asymmetric volume fraction $(f_{\rm p}\approx 0.41)$. At 180 °C, the segregation strength of PES18Li is $\chi N_{\rm v}\approx 20.0$, which is consistent with a HEX morphology, *i.e.*, being self-assembled

Scheme 1. Experimentally obtained Flory–Huggins interaction parameters (χ) and the minimum domain spacings (d_{\min}) for various block copolymer architectures. The low- χ and high-N diblock copolymers are represented by the poly(styrene-b-methyl methacrylate). The values for high- χ and low-N diblock copolymers are obtained from the poly(styrene-b-acrylic acid). The PESxLi polymers indicate the ultrahigh- χ and low-N multiblock copolymers. All χ parameters are determined from the scattering intensity of disordered melts using mean-field theory and are shown for the values at 25 °C and reference volume of 118 Å³.



into the ordered morphologies. Regarding the value of R_g , the radius of gyration of repeating unit in disordered PES12Li is \sim 8.2 Å at all measured temperatures (Table S1). In comparison, a Monte Carlo simulation approximates the radius of gyration of 18-carbon polyethylene chains as 5.3 Å.⁶⁴ Here, the larger radius of gyration in the PES12Li polymer is attributed to the rigid polar ionic blocks and bulky Li⁺SO₃⁻ that increases the radial distance between the repeating units. Thus, the results obtained from the random phase approximation for multiblock copolymers are consistent with the physical properties of PESxLi polymers.

In Figure 4, experimentally observed phase transitions of PESxLi polymers are displayed in the χN versus f_p diagram, along with the order-to-order transition (OOT) and order-todisorder transition (ODT) boundaries numerically calculated from the self-consistent field theory (SCFT). The calculations used the open-source of polymer self-consistent field (PSCF) code; details of running the PSCF code and explanations of the methodology are provided elsewhere. 65 Here, we identify the equilibrium morphologies of LAY, GYR, and HEX as a function of χN and f_p for $(AB)_{17}$ multiblock copolymers (see the Supporting Information). These phase boundaries are consistent with previously reported results for (AB), multiblocks to within $f_p < 0.005$ due to our use of finite n = 17.66Note that we omitted other equilibrium morphologies, such as a sphere (bcc) and O70 (Fddd), because they were not observed in PESxLi polymers. Unsurprisingly, the experimental OOTs and ODT of PESxLi polymers do not match the theoretical calculations. Specifically, the GYR-HEX (PES23Li and PES18Li) and LAY-DIS (PES12Li) transitions are shifted to lower f_p as compared to the theoretical phase boundaries. Also, the magnitude of this boundary shift increases with a higher volume asymmetry of the blocks, i.e., lower f_p . Therefore, Figure 4 shows that the SCFT calculations for conformationally symmetric and Gaussian chain of neutral multiblock copolymers are inconsistent with the equilibrium morphologies experimentally observed in PESxLi ion-containing multiblock copolymers.

These discrepancies between the phase boundaries of PESxLi polymers and the SCFT can likely be attributed to the presence of charged species on the polymer backbone. A hybrid self-consistent field theory and liquid state integral equation theory (SCFT-LS) demonstrates that the presence of charged blocks significantly skews the phase boundaries as a function of charge fraction and Coulombic interaction

strengths.⁴¹ The SCFT-LS predicts the shift of phase boundaries toward a lower volume fraction of the charged blocks, which is consistent with the shift observed for PESxLi polymers (Figure 4). Also, dissipative particle dynamics (DPD) simulations show the shift of phase boundaries with an increasing charge fraction.⁴³ Therefore, the SCFT-LS theory and DPD simulations applied to charged multiblock architecture might provide additional insights regarding the role of charges on the phase behaviors of PESxLi polymers.

In addition, asymmetry of statistical lengths of the blocks can shift the phase boundaries of block copolymers compared to the conformationally symmetric block copolymers. The SCFT calculations of conformationally symmetric and asymmetric neutral diblock copolymers show that the phase boundaries shift toward a lower volume fraction of the shorter statistical block length. Finally, low-N polymer chains shift the phase boundaries upward compared to the longer polymers with Gaussian chain conformations. This low-N effect is mainly due to the entropic penalty of short chains and is demonstrated by the modified SCFT model for discrete chains. Since these physical attributes were studied with neutral block copolymers, it is now important to understand the asymmetric statistical lengths and low-N effects within charged block copolymers.

Scheme 1 highlights a design strategy for generating sub-3nm features by using ultrahigh-\(\chi\) and low-N multiblock copolymers. To overcome the limitation of conventional low- χ and high-N diblock copolymers (e.g., poly(styrene-b-methyl methacrylate)), many studies have focused on designing high-y and low-N diblock copolymers. For poly(styrene-b-acrylic acid) diblock copolymers, $\chi(25~^{\circ}\text{C}) \approx 0.885$ is obtained with a minimum layer spacing of 6.9 nm. 52 Notably, PESxLi multiblock copolymers containing highly incompatible polar ionic and nonpolar polyethylene blocks exhibit an ultrahigh χ $(25 \text{ °C}) \approx 3.21$ and sub-3-nm domain spacings. Here, ultrahigh χ produces phase separation in short blocks, while a multiblock architecture further reduces domain spacings. For example, SCFT calculations show that the layer spacing of (AB)₁₇ multiblock copolymers drops 68% relative to the layer spacing of AB diblock copolymers (Figure S8).

In summary, the PES α Li multiblock copolymers achieve sub-3-nm domain spacings *via* three design criteria. (1) Highly incompatible polar ionic and nonpolar blocks segregate even when the alternating blocks contain just 18–29 backbone atoms. (2) The increased number of repeating subunits (n), namely, a multiblock architecture, $(AB)_n$, reduces the domain

spacing relative to an AB diblock architecture. (3) Step-growth polymerization is advantageous for designing high- χ and low-N multiblock polymers with exceptional control over the block lengths. Note that when n > 20, the domain spacing is insensitive to the total polymer molecular weight and molecular weight dispersity. Moreover, the application of alternating multiblock copolymers synthesized via step-growth polymers for nanolithography significantly expands the range of chemical species to provide patterning contrast. Thus, this study of PESxLi polymers provides an initial step toward designing ultrahigh- χ and low-N multiblock copolymers for nanopatterning.

CONCLUSION

We demonstrate ordered morphologies with sub-3-nm domain spacings in a multiblock copolymer with an ultrahigh Flory-Huggins interaction parameter (χ) and short block lengths (N). As a function of temperature, PES18Li exhibits layered, gyroid, and hexagonal morphologies with sub-3-nm domain spacings, while PES12Li shows a layer-to-disorder transition at ~110 °C. The value of χ is determined from the disordered morphologies of PES12Li using mean-field theory with the reference volume of 118 Å³: $\chi(T) = 77.4/T + 2.95$ (*T* in Kelvin). This yields $\chi(25~^{\circ}\text{C}) \approx 3.21$, which is one of the largest values reported for block copolymers. The experimental phase transitions of PESxLi are inconsistent with the selfconsistent field theory, presumably due to the presence of ionic groups and the short blocks. Clearly, more work is needed to develop the theoretical predictions of phase behavior in strongly phase-separated multiblock copolymers, particularly when the polymer has pendant ionic groups. Theoretical understanding combined with various polymer chemistries via step-growth polymerization will advance the ability to design and tune self-assembled nanoscale morphologies.

Such ordered phases at sub-3-nm length scales open various lines of inquiry for nanotechnology. For example, these or similar step-grown multiblock copolymers should be explored for nanolithography building upon the strategies developed for diblock copolymers. By directly employing suitable functional groups or by a chemical amplification step, these multiblock copolymer thin films self-assembled in nanostructures should be pattern-transferable. Alternatively, the ordered morphologies in these multiblock copolymers may provide an opportunity to study the optical properties in sub-3-nm nanostructures, including controlling the refractive index in multilayered materials or designing metamaterials (*e.g.*, gyroid optical metastructures). Finally, these precisely segmented multiblock copolymers could also be used to template 2D materials, nanoparticles, or nanoporous materials.

METHODS

Synthesis of Materials. All reactions described were performed under an inert gas atmosphere using standard glovebox and Schlenk techniques. LiCl was supplied by Merck. Dialysis tubes by SpectraPor were supplied by Carl Roth and used for purification of the polymers (3.5 kDa pore size, 54 mm broadness). To obtain the PESxLi materials, the corresponding PESxNBu₄ polymers with tetra-*n*-butylammonium counterions (NBu₄) were synthesized according to a previously reported procedure.

For PES12Li, the polymer PES12NBu₄ (2 g) was dissolved in an aqueous LiCl solution (2 M, 50 mL) and methanol (50 mL). The solution was dialyzed for 3 days (5 L of deionized water bath, exchange water 3×/day). The solvent was removed by lyophilization, and NMR measurement ensured the absence of tetra-n-butylammo-

nium counterions. The process was repeated until no tetra-*n*-butylammonium remained. PES12Li was obtained in 80% yield (0.98 g).

For PES18Li, the polymer PES18NBu₄ (3.1 g) was dissolved in an aqueous LiCl solution (2 M, 100 mL). The polymer started to precipitate as a white solid after vigorous stirring. The precipitate was filtered off and washed with deionized water until no precipitate formed from the filtrate by the addition of AgNO₃ in water (0.01 M). The polymer was washed with acetone to facilitate the drying process. The polymer was dried in a vacuum drying oven at 3 mbar for 3 days and was obtained in 65% yield (1.36 g).

Gel Permeation Chromatography (GPC). The polydispersity indexes of PES12Li and PES18Li were determined by GPC using dimethylformamide (DMF) eluent. The GPC system is equipped with a Waters 1515 isocratic pump, a Waters 2707 autosampler, a Waters 2414 differential refractive index detector, and three Polymer Standards Service GRAM columns (two 1000 Å porosity columns and one 30 Å porosity column with $10~\mu m$ particle size). The DMF eluent contained 0.1 wt % LiBr, and the flow rate was 1~mL/min. The polystyrene standards over a range of 1000 to 1000 000 g/mol were used for the calibration.

Nuclear Magnetic Resonance (NMR) Spectroscopy. The characterization of the soluble intermediate products by NMR spectroscopy was performed in dimethyl sulfoxide- d_6 as solvent at 110 °C. A Bruker Avance III HD 400 spectrometer with a TBO probe with Z-gradient was used. ¹H chemical shifts were referenced to the solvent signal (residual proton signal). Multiplicities are reported as follows: s (singlet), d (doublet), t (triplet), m (multiplet), v (virtual), and combinations thereof. MestreNova software by Mestrelab Research S.L. was used for the evaluation of NMR data. Deuterated solvents used for NMR spectroscopy were supplied by Eurisotop.

X-ray Scattering Experiments. X-ray scattering experiments were performed in the Dual-source and Environmental X-ray Scattering (DEXS) facility at the University of Pennsylvania. The DEXS facility is equipped with a PILATUS 1 M detector for smallangle scattering, a PILATUS 100 K detector for wide-angle scattering, and a GeniX3D beam source (8 keV, Cu K α , λ = 1.54 Å). Dried polymer samples (24 h, $T_{\rm m}$ + 20 °C, vacuum) were sealed in 1.0 mm diameter glass capillaries, and 2D scattering data were collected every 10 °C for 10 min, after 15 min equilibration. The heating and cooling rates were 10 °C/min. The scattering data were isotropic and integrated into I(q) plots. Small- and wide-angle plots were arbitrarily shifted in I(q) to display the scattering data at 0.1 Å⁻¹ < q < 1.8 Å⁻¹. The absolute scattering intensities of disordered PES12Li were determined by using a glassy carbon standard. The absolute scattering data were collected every 10 °C for 10 min after 15 min equilibration, and scattering profiles were identical for heating and cooling.

Differential Scanning Calorimetry (DSC). DSC experiments were performed with a TA Instruments DSC Q2000. The freeze-dried polymer samples were dried at 150 °C under vacuum prior to performing DSC measurements. Samples were measured at a 3 °C/min ramping rate under a nitrogen atmosphere.

ASSOCIATED CONTENT

Solution Supporting Information

The Supporting Information is available free of charge at https://pubs.acs.org/doi/10.1021/acsnano.1c06734.

GPC data, ¹H NMR spectrum, full *in situ* X-ray scattering data, DSC thermograms, X-ray scattering of PES12Li after isothermal annealing at 90 °C, scattering profiles of disordered PES12Li, best fit of eq 1 and fitting parameters, the ratio of layer spacing of (AB)_n multiblock copolymers to the diblock copolymers calculated from the self-consistent field theory (PDF)

AUTHOR INFORMATION

Corresponding Author

Karen I. Winey — Department of Materials Science and Engineering, University of Pennsylvania, Philadelphia, Pennsylvania 19104, United States; oorcid.org/0000-0001-5856-3410; Email: winey@seas.upenn.edu

Authors

Jinseok Park — Department of Materials Science and Engineering, University of Pennsylvania, Philadelphia, Pennsylvania 19104, United States; orcid.org/0000-0002-0389-9707

Anne Staiger – Department of Chemistry, University of Konstanz, 78457 Konstanz, Germany; orcid.org/0000-0002-6103-4402

Stefan Mecking – Department of Chemistry, University of Konstanz, 78457 Konstanz, Germany; orcid.org/0000-0002-6618-6659

Complete contact information is available at: https://pubs.acs.org/10.1021/acsnano.1c06734

Notes

The authors declare no competing financial interest.

ACKNOWLEDGMENTS

J.P. and K.I.W. acknowledge funding by the National Science Foundation (DMR 1904767). J.P. and K.I.W. also acknowledge NSF MRSEC (17-20530), NSF MRI (17-25969), and ARO DURIP grants (W911NF-17-1-0282) for the Dual Source and Environmental X-ray Scattering facility operated by the Laboratory for Research on the Structure of Matter at the University of Pennsylvania. J.P. acknowledges a graduate student fellowship from the Vagelos Institute for Energy Science and Technology at the University of Pennsylvania. J.P. acknowledges NSF PIRE (15-45884) for the writing workshop. A.S. and S.M. gratefully acknowledge funding by the Baden-Württemberg Foundation (project "PRICON"). We acknowledge NSF DMR 1719875 for the use of GPC equipment in Cornell Center for Materials Research at Cornell University. We thank Chinedum Osuji and Amalie L. Frischknecht for the helpful discussions.

REFERENCES

- (1) Chai, J.; Wang, D.; Fan, X.; Buriak, J. M. Assembly of Aligned Linear Metallic Patterns on Silicon. *Nat. Nanotechnol.* **200**7, 2, 500–506
- (2) Thurn-Albrecht, T.; Schotter, J.; Kastle, G. A.; Emley, N.; Shibauchi, T.; Krusin-Elbaum, L.; Guarini, K.; Black, C. T.; Tuominen, M. T.; Russell, T. P. Ultrahigh-Density Nanowire Arrays Grown in Self-Assembled Diblock Copolymer Templates. *Science* (Washington, DC, U. S.) 2000, 290, 2126–2129.
- (3) Shin, D. O.; Lee, D. H.; Moon, H. S.; Jeong, S. J.; Kim, J. Y.; Mun, J. H.; Cho, H.; Park, S.; Kim, S. O. Sub-Nanometer Level Size Tuning of a Monodisperse Nanoparticle Array via Block Copolymer Lithography. *Adv. Funct. Mater.* **2011**, *21*, 250–254.
- (4) Park, M.; Harrison, C.; Chaikin, P. M.; Register, R. A.; Adamson, D. H. Block Copolymer Lithography: Periodic Arrays of ~ 1011 Holes in 1 Square Centimeter. *Science (Washington, DC, U. S.)* 1997, 276, 1401–1404.
- (5) Chan, V. Z. H.; Hoffman, J.; Lee, V. Y.; Iatrou, H.; Avgeropoulos, A.; Hadjichristidis, N.; Miller, R. D.; Thomas, E. L. Ordered Bicontinuous Nanoporous and Nanorelief Ceramic Films from Serf Assembling Polymer Precursors. *Science (Washington, DC, U. S.)* 1999, 286, 1716–1719.

- (6) Zhou, C.; Segal-Peretz, T.; Oruc, M. E.; Suh, H. S.; Wu, G.; Nealey, P. F. Fabrication of Nanoporous Alumina Ultrafiltration Membrane with Tunable Pore Size Using Block Copolymer Templates. *Adv. Funct. Mater.* **2017**, 27, 19–22.
- (7) Zhang, Y.; Dong, R.; Gabinet, U. R.; Poling-Skutvik, R.; Kim, N. K.; Lee, C.; Imran, O. Q.; Feng, X.; Osuji, C. O. Rapid Fabrication by Lyotropic Self-Assembly of Thin Nanofiltration Membranes with Uniform 1 Nanometer Pores. ACS Nano 2021, 15, 8192–8203.
- (8) Leong, M.; Doris, B.; Kedzierski, J.; Rim, K.; Yang, M. Silicon Device Scaling to the Sub-10-Nm Regime. *Science (Washington, DC, U. S.)* **2004**, 306, 2057–2060.
- (9) Suh, H. S.; Kim, D. H.; Moni, P.; Xiong, S.; Ocola, L. E.; Zaluzec, N. J.; Gleason, K. K.; Nealey, P. F. Sub-10-Nm Patterning via Directed Self-Assembly of Block Copolymer Films with a Vapour-Phase Deposited Topcoat. *Nat. Nanotechnol.* **2017**, *12*, 575–581.
- (10) Kim, J. Y.; Kim, H.; Kim, B. H.; Chang, T.; Lim, J.; Jin, H. M.; Mun, J. H.; Choi, Y. J.; Chung, K.; Shin, J.; Fan, S.; Kim, S. O. Highly Tunable Refractive Index Visible-Light Metasurface from Block Copolymer Self-Assembly. *Nat. Commun.* **2016**, *7*, 1–9.
- (11) Dolan, J. A.; Wilts, B. D.; Vignolini, S.; Baumberg, J. J.; Steiner, U.; Wilkinson, T. D. Optical Properties of Gyroid Structured Materials: From Photonic Crystals to Metamaterials. *Adv. Opt. Mater.* **2015**, *3*, 12–32.
- (12) Yun, T.; Jin, H. M.; Kim, D. H.; Han, K. H.; Yang, G. G.; Lee, G. Y.; Lee, G. S.; Choi, J. Y.; Kim, I. D.; Kim, S. O. 2D Metal Chalcogenide Nanopatterns by Block Copolymer Lithography. *Adv. Funct. Mater.* **2018**, 28, 1–8.
- (13) Fiori, G.; Bonaccorso, F.; Iannaccone, G.; Palacios, T.; Neumaier, D.; Seabaugh, A.; Banerjee, S. K.; Colombo, L. Electronics Based on Two-Dimensional Materials. *Nat. Nanotechnol.* **2014**, *9*, 768–779.
- (14) Chia, X.; Eng, A. Y. S.; Ambrosi, A.; Tan, S. M.; Pumera, M. Electrochemistry of Nanostructured Layered Transition-Metal Dichalcogenides. *Chem. Rev.* **2015**, *115*, 11941–11966.
- (15) Kim, J. H.; Jin, H. M.; Yang, G. G.; Han, K. H.; Yun, T.; Shin, J. Y.; Jeong, S. J.; Kim, S. O. Smart Nanostructured Materials Based on Self-Assembly of Block Copolymers. *Adv. Funct. Mater.* **2020**, *30*, 1–15
- (16) Sinturel, C.; Bates, F. S.; Hillmyer, M. A. High χ -Low N Block Polymers: How Far Can We Go? *ACS Macro Lett.* **2015**, *4*, 1044–1050.
- (17) Ruiz, R.; Kang, H.; Detcheverry, F. A.; Dobisz, E.; Kercher, D. S.; Albrecht, T. R.; De Pablo, J. J.; Nealey, P. F. Density Multiplication and Improved Lithography by Directed Block Copolymer Assembly. *Science (Washington, DC, U. S.)* **2008**, *321*, 936–939.
- (18) Leibler, L. Theory of Microphase Separation in Block Copolymers. *Macromolecules* **1980**, *13*, 1602–1617.
- (19) Semenov, A. N. Contribution to the Theory of Microphase Layering in Block-Copolymer Melts. *Zh. Eksp. Teor. Fiz* **1985**, *88*, 1242–1256.
- (20) Matsen, M. W.; Bates, F. S. Unifying Weak- and Strong-Segregation Block Copolymer Theories. *Macromolecules* **1996**, *29*, 1091–1098.
- (21) Matsen, M. W.; Whitmore, M. D. Accurate Diblock Copolymer Phase Boundaries at Strong Segregations. *J. Chem. Phys.* **1996**, *105*, 9698–9701.
- (22) Sweat, D. P.; Kim, M.; Schmitt, A. K.; Perroni, D. V.; Fry, C. G.; Mahanthappa, M. K.; Gopalan, P. Phase Behavior of Poly(4-Hydroxystyrene-Block-Styrene) Synthesized by Living Anionic Polymerization of an Acetal Protected Monomer. *Macromolecules* **2014**, *47*, 6302–6310.
- (23) Kwak, J.; Mishra, A. K.; Lee, J.; Lee, K. S.; Choi, C.; Maiti, S.; Kim, M.; Kim, J. K. Fabrication of Sub-3 Nm Feature Size Based on Block Copolymer Self-Assembly for Next-Generation Nanolithography. *Macromolecules* **2017**, *50*, 6813–6818.
- (24) Azuma, K.; Sun, J.; Choo, Y.; Rokhlenko, Y.; Dwyer, J. H.; Schweitzer, B.; Hayakawa, T.; Osuji, C. O.; Gopalan, P. Self-Assembly of an Ultrahigh-χ Block Copolymer with Versatile Etch Selectivity. *Macromolecules* **2018**, *51*, 6460–6467.

- (25) Hirai, T.; Leolukman, M.; Liu, C. C.; Han, E.; Kim, Y. J.; Ishida, Y.; Hayakawa, T.; Kakimoto, M. A.; Nealey, P. F.; Gopalan, P. One-Step Direct-Patterning Template Utilizing Self-Assembly of POSS-Containing Block Copolymers. *Adv. Mater.* **2009**, *21*, 4334–4338.
- (26) Nakatani, R.; Takano, H.; Chandra, A.; Yoshimura, Y.; Wang, L.; Suzuki, Y.; Tanaka, Y.; Maeda, R.; Kihara, N.; Minegishi, S.; Miyagi, K.; Kasahara, Y.; Sato, H.; Seino, Y.; Azuma, T.; Yokoyama, H.; Ober, C. K.; Hayakawa, T. Perpendicular Orientation Control without Interfacial Treatment of RAFT-Synthesized High-χ Block Copolymer Thin Films with Sub-10 Nm Features Prepared via Thermal Annealing. ACS Appl. Mater. Interfaces 2017, 9, 31266—31278.
- (27) Wang, C.; Li, X.; Deng, H. Synthesis of a Fluoromethacrylate Hydroxystyrene Block Copolymer Capable of Rapidly Forming Sub-5 Nm Domains at Low Temperatures. *ACS Macro Lett.* **2019**, *8*, 368–373.
- (28) Jo, S.; Jeon, S.; Jun, T.; Park, C.; Ryu, D. Y. Fluorine-Containing Styrenic Block Copolymers toward High χ and Perpendicular Lamellae in Thin Films. *Macromolecules* **2018**, *51*, 7152–7159.
- (29) Yue, Z.; Sivaniah, E.; Hashimoto, T. SAXS Analysis of the Order-Disorder Transition and the Interaction Parameter of Polystyrene-Block-Poly(methyl Methacrylate). *Macromolecules* **2008**, *41*, 9948–9951.
- (30) Bates, F. S.; Hillmyer, M. a.; Lodge, T. P.; Bates, C. M.; Delaney, K. T.; Fredrickson, G. H. Multiblock Polymers: Panacea or Pandora's Box. *Science (Washington, DC, U. S.)* **2012**, *336*, 434–440.
- (31) Wu, L.; Cochran, E. W.; Lodge, T. P.; Bates, F. S. Consequences of Block Number on the Order-Disorder Transition and Viscoelastic Properties of Linear (AB)n Multiblock Copolymers. *Macromolecules* **2004**, *37*, 3360–3368.
- (32) Steube, M.; Johann, T.; Galanos, E.; Appold, M.; Rüttiger, C.; Mezger, M.; Gallei, M.; Müller, A. H. E.; Floudas, G.; Frey, H. Isoprene/Styrene Tapered Multiblock Copolymers with up to Ten Blocks: Synthesis, Phase Behavior, Order, and Mechanical Properties. *Macromolecules* **2018**, *51*, 10246–10258.
- (33) Li, S.; Xu, Q.; Li, K.; Yu, C.; Zhou, Y. High-χ Alternating Copolymers for Accessing Sub-5 Nm Domains via Simulations. *Phys. Chem. Chem. Phys.* **2020**, 22, 5577–5583.
- (34) Smith, S. D.; Spontak, R. J.; Satkowski, M. M.; Ashraf, A.; Heape, A. K.; Lin, J. S. Microphase-Separated Poly(styrene-b-Isoprene)n Multiblock Copolymers with Constant Block Lengths. *Polymer* 1994, 35, 4527–4536.
- (35) Funt, J. M.; Magill, J. H. Thermal Decomposition of Polystyrene: Effect of Molecular Weight. *J. Polym. Sci., Polym. Phys. Ed.* 1974, 12, 217–220.
- (36) Nunes, R. W.; Martin, J. R.; Johnson, J. F. Influence of Molecular Weight and Molecular Weight Distribution on Mechanical Properties of Polymers. *Polym. Eng. Sci.* **1982**, 22, 205–228.
- (37) Anderson, T. G.; Bersted, B. H. Influence of Molecular Weight and Molecular Weight Distribution on the Tensile Properties of Amorphous Polymers. *J. Appl. Polym. Sci.* **1990**, *39*, 499–514.
- (38) Benoit, H.; Hadziioannou, G. Scattering Theory and Properties of Block Copolymers with Various Architectures in the Homogeneous Bulk State. *Macromolecules* **1988**, *21*, 1449–1464.
- (39) Kavassalis, T. A.; Whitmore, M. D. On the Theory of Linear Multiblock Copolymers. *Macromolecules* **1991**, *24*, 5340–5345.
- (40) Zielinski, J. M.; Spontak, R. J. Confined Single-Chain Model of Microphase-Separated Multiblock Copolymers. 1. (AB)n Copolymers. *Macromolecules* **1992**, *25*, 653–662.
- (41) Sing, C. E.; Zwanikken, J. W.; Olvera De La Cruz, M. Electrostatic Control of Block Copolymer Morphology. *Nat. Mater.* **2014**, *13*, 694–698.
- (42) Luo, Y.; Montarnal, D.; Treat, N. J.; Hustad, P. D.; Christianson, M. D.; Kramer, E. J.; Fredrickson, G. H.; Hawker, C. J. Enhanced Block Copolymer Phase Separation Using Click Chemistry and Ionic Junctions. *ACS Macro Lett.* **2015**, *4*, 1332–1336. (43) Zhai, C.; Zhou, H.; Gao, T.; Zhao, L.; Lin, S. Electrostatically Tuned Microdomain Morphology and Phase-Dependent Ion Trans-

- port Anisotropy in Single-Ion Conducting Block Copolyelectrolytes. *Macromolecules* **2018**, *51*, 4471–4483.
- (44) Li, W.; Carrillo, J. M. Y.; Sumpter, B. G.; Kumar, R. Modulating Microphase Separation of Lamellae-Forming Diblock Copolymers via Ionic Junctions. *ACS Macro Lett.* **2020**, *9*, 1667–1673.
- (45) Park, J.; Staiger, A.; Mecking, S.; Winey, K. I. Structure Property Relationships in Single-Ion Conducting Multiblock Copolymers: A Phase Diagram and Ionic Conductivities. *Macromolecules* **2021**, *54*, 4269–4279.
- (46) Yan, L.; Rank, C.; Mecking, S.; Winey, K. I. Gyroid and Other Ordered Morphologies in Single-Ion Conducting Polymers and Their Impact on Ion Conductivity. *J. Am. Chem. Soc.* **2020**, *142*, 857–866.
- (47) Rank, C.; Yan, L.; Mecking, S.; Winey, K. I. Periodic Polyethylene Sulfonates from Polyesterification: Bulk and Nanoparticle Morphologies and Ionic Conductivities. *Macromolecules* **2019**, 52, 8466–8475.
- (48) Tashiro, K.; Sasaki, S.; Kobayashi, M. Structural Investigation of Orthorhombic-to-Hexagonal Phase Transition in Polyethylene Crystal: The Experimental Confirmation of the Conformationally Disordered Structure by X-Ray Diffraction and Infrared/Raman Spectroscopic Measurements. *Macromolecules* **1996**, 29, 7460–7469.
- (49) Sakamoto, N.; Hashimoto, T. Order-Disorder Transition of Low Molecular Weight Polystyrene-Block-Polyisoprene. 1. SAXS Analysis of Two Characteristic Temperatures. *Macromolecules* 1995, 28, 6825–6834.
- (50) Bates, F. S.; Rosedale, J. H.; Fredrickson, G. H. Fluctuation Effects in a Symmetric Diblock Copolymer near the Order-Disorder Transition. *J. Chem. Phys.* **1990**, *92*, *6255–6270*.
- (51) Fredrickson, G. H.; Helfand, E. Fluctuation Effects in the Theory of Microphase Separation in Block Copolymers. *J. Chem. Phys.* **1987**, *87*, 697–705.
- (52) Yu, D. M.; Smith, D. M.; Kim, H.; Rzayev, J.; Russell, T. P. Two-Step Chemical Transformation of Polystyrene- Block-Poly(solketal Acrylate) Copolymers for Increasing χ . *Macromolecules* **2019**, 52, 6458–6466.
- (53) Rodwogin, M. D.; Spanjers, C. S.; Leighton, C.; Hillmyer, M. A. Polylactide-Poly(dimethylsiloxane)-Polylactide Triblock Copolymers as Multifunctional Materials for Nanolithographic Applications. *ACS Nano* **2010**, *4*, 725–732.
- (54) Chintapalli, M.; Timachova, K.; Olson, K. R.; Mecham, S. J.; Desimone, J. M.; Balsara, N. P. Lithium Salt Distribution and Thermodynamics in Electrolytes Based on Short Perfluoropolyether-Block-Poly(ethylene Oxide) Copolymers. *Macromolecules* **2020**, 53, 1142–1153
- (55) Nakamura, I.; Wang, Z. G. Salt-Doped Block Copolymers: Ion Distribution, Domain Spacing and Effective χ Parameter. *Soft Matter* **2012**, *8*, 9356–9367.
- (56) Nakamura, I.; Wang, Z. G. Thermodynamics of Salt-Doped Block Copolymers. ACS Macro Lett. **2014**, *3*, 708–711.
- (57) Son, C. Y.; Wang, Z. G. Ion Transport in Small-Molecule and Polymer Electrolytes. *J. Chem. Phys.* **2020**, *153*, 100903.
- (58) Brown, J. R.; Seo, Y.; Hall, L. M. Ion Correlation Effects in Salt-Doped Block Copolymers. *Phys. Rev. Lett.* **2018**, *120*, 127801.
- (59) Loo, W. S.; Galluzzo, M. D.; Li, X.; Maslyn, J. A.; Oh, H. J.; Mongcopa, K. I.; Zhu, C.; Wang, A. A.; Wang, X.; Garetz, B. A.; Balsara, N. P. Phase Behavior of Mixtures of Block Copolymers and a Lithium Salt. *J. Phys. Chem. B* **2018**, *122*, 8065–8074.
- (60) Loo, W. S.; Sethi, G. K.; Teran, A. A.; Galluzzo, M. D.; Maslyn, J. A.; Oh, H. J.; Mongcopa, K. I.; Balsara, N. P. Composition Dependence of the Flory-Huggins Interaction Parameters of Block Copolymer Electrolytes and the Isotaksis Point. *Macromolecules* **2019**, *52*, *5590*–*5601*.
- (61) Teran, A. A.; Balsara, N. P. Thermodynamics of Block Copolymers with and without Salt. *J. Phys. Chem. B* **2014**, *118*, 4–17. (62) Wanakule, N. S.; Virgili, J. M.; Teran, A. A.; Wang, Z. G.; Balsara, N. P. Thermodynamic Properties of Block Copolymer Electrolytes Containing Imidazolium and Lithium Salts. *Macromolecules* **2010**, *43*, 8282–8289.

- (63) Hou, K. J.; Loo, W. S.; Balsara, N. P.; Qin, J. Comparing Experimental Phase Behavior of Ion-Doped Block Copolymers with Theoretical Predictions Based on Selective Ion Solvation. *Macromolecules* **2020**, *53*, 3956–3966.
- (64) Baschanagel, J.; Qin, K.; Paul, W.; Binder, K. Monte Carlo Simulation of Models for Single Polyethylene Coils. *Macromolecules* **1992**, 25, 3114–3124.
- (65) Arora, A.; Qin, J.; Morse, D. C.; Delaney, K. T.; Fredrickson, G. H.; Bates, F. S.; Dorfman, K. D. Broadly Accessible Self-Consistent Field Theory for Block Polymer Materials Discovery. *Macromolecules* **2016**, *49*, 4675–4690.
- (66) Matsen, M. W. Effect of Architecture on the Phase Behavior of AB-Type Block Copolymer Melts. *Macromolecules* **2012**, *45*, 2161–2165.
- (67) Matsen, M. W. Field Theoretic Approach for Block Polymer Melts: SCFT and FTS. J. Chem. Phys. 2020, 152, 110901.
- (68) Matsen, M. W. Self-Consistent Field Theory for Melts of Low-Molecular-Weight Diblock Copolymer. *Macromolecules* **2012**, 45, 8502–8509.